

Cross-modal learning for plankton recognition

Joona Kareinen¹[0009-0005-5997-2327], Veikka Immonen¹, Tuomas Eerola¹[0000-0003-1352-0999], Lumi Haraguchi²[0000-0001-6307-1808], Lasse Lensu¹[0000-0002-7691-121X], Kaisa Kraft²[0000-0001-6290-3887], Sanna Suikkanen²[0000-0002-0768-8149], and Heikki Kälviäinen^{1,3}[0000-0002-0790-6847]

¹ Lappeenranta-Lahti University of Technology LUT, Lappeenranta, Finland

² Finnish Environment Institute, Helsinki, Finland

³ Faculty of Information Technology, Brno University of Technology, Czechia

Abstract. This paper considers self-supervised cross-modal coordination as a strategy enabling utilization of multiple modalities and large volumes of unlabeled plankton data to build models for plankton recognition. Automated imaging instruments facilitate the continuous collection of plankton image data on a large scale. Current methods for automatic plankton image recognition rely primarily on supervised approaches, which require labeled training sets that are labor-intensive to collect. On the other hand, some modern plankton imaging instruments complement image information with optical measurement data, such as scatter and fluorescence profiles, which currently are not widely utilized in plankton recognition. In this work, we explore the possibility of using such measurement data to guide the learning process without requiring manual labeling. Inspired by the concepts behind Contrastive Language-Image Pre-training (CLIP), we train encoders for both modalities using only binary supervisory information indicating whether a given image and profile originate from the same particle or from different particles. For plankton recognition, we employ a small labeled gallery of known plankton species combined with a k -NN classifier. This approach yields a recognition model that is inherently multimodal, i.e., capable of utilizing information extracted from both image and profile data. We demonstrate that the proposed method achieves high recognition accuracy while requiring only a minimal number of labeled images. Furthermore, we show that the approach outperforms an image-only self-supervised baseline. Code available at <https://github.com/Jookare/cross-modal-plankton>.

Keywords: plankton recognition · multimodal learning · coordinated representation

1 Introduction

Plankton play a fundamental role in sustaining life on Earth, contributing ca. 50% of global oxygen and ca. 40% of carbon fixation, forming the base of aquatic

food webs, and serving as sensitive indicators of environmental change [11,12]. As climate change and pollution increasingly impact aquatic ecosystems, monitoring plankton communities can provide early warnings of ecological disruption. Yet, despite their importance, plankton communities remain poorly understood due to their rapid turnover and sensitivity to environmental changes.

Over the past decades, technological advancements have led to the development of several automated plankton imaging instruments that combine microscopy with digital cameras to produce high-quality images at relatively low operational costs. These devices enable large-scale data collection, generating millions of plankton images across different aquatic environments [14, 22, 28]. However, manual annotation at such a scale is infeasible, as expert annotation of plankton images is both expensive and time-consuming. To address this limitation, various computer vision-based plankton recognition methods have been developed [8].

Most existing plankton recognition methods rely on a single modality of data, typically images. While image-based models have achieved accurate results, they are inherently limited by image quality, subtle inter-species differences, and incomplete class coverage in labeled datasets [8]. Some plankton imaging instruments, however, provide additional data beyond images, such as optical measurements (e.g., scatter and fluorescence profiles), or are associated with contextual metadata (e.g., sampling location, water temperature, and time) [7]. Some instruments, like pulse-shape recording and imaging flow cytometer CytoSense [7, 14], rely on the optical measurements as their primary modality, which is recorded for each particle, and the images are taken as supplementary to help connect the optical measurements with taxonomical units. Although these additional or auxiliary modalities contain complementary information about both individual particles and entire samples, they are underutilized in existing recognition approaches. Data composed primarily of optical information is also more challenging for existing models to recognize. The existence of this additional data creates an opportunity for multimodal learning, where recognition models leverage multiple data types simultaneously or interchangeably, potentially improving both accuracy and robustness.

Perhaps even more notably, the auxiliary data can be used to guide self-supervised learning, thereby reducing the need for labor-intensive expert labeling. Cross-modal learning techniques, such as Contrastive Language-Image Pre-training (CLIP) [29] align representations across modalities, enabling classification or retrieval without class labels. This characteristic makes the use of multiple modalities particularly compelling: each particle is described by complementary signals that provide a richer representation than image data alone. At the same time, it allows to take advantage of the large volumes of unlabeled data produced by modern imaging instruments for model training.

In this paper, we study cross-modal learning for plankton recognition, focusing specifically on data collected using CytoSense [7, 14], which includes both bright-field images and optical profiles of individual particles. We aim to address three key research questions: (1) Is it possible to obtain image and profile em-

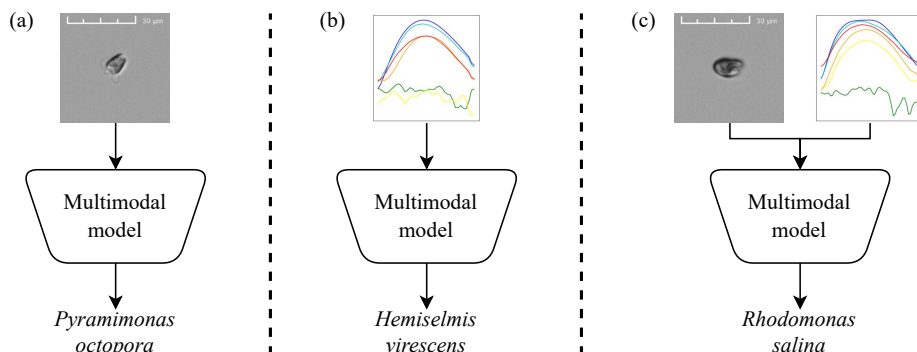


Fig. 1: Overview of the proposed multimodal plankton recognition model for CytoSense capable of classifying plankton species using (a) only bright-field images, (b) only optical profiles, or (c) both at the same time.

beddings suitable for plankton recognition using cross-modal learning without relying on class labels? (2) Can plankton recognition be improved by incorporating an additional modality? (3) How well does the framework perform with only the non-image data? To answer these questions, and inspired by CLIP, we propose a contrastive pre-training approach that aligns paired image–profile samples in a shared embedding space. For plankton recognition, we introduce a method that uses small, labeled gallery of known plankton species and performs nearest neighbor search in the embedding space. This recognition method allows either modality to be used independently or both modalities to be combined for improved performance (see Fig. 1).

In the experimental section, we demonstrate that the proposed method not only achieves high plankton recognition accuracy when training and test data come from the same dataset (in-domain) but also generalizes well to different datasets with varying class distributions (cross-domain). Furthermore, we show that the method outperforms the image-only self-supervised learning baseline DINO [4].

The main contributions of this study are as follows: (1) a multimodal plankton recognition framework for CytoSense data that combines bright-field images and optical profiles, (2) a new publicly available multimodal plankton dataset, SYKE-plankton_CytoSense_2025 [19], and (3) a label-free contrastive cross-modal learning strategy, accompanied with an analysis of how different modalities contribute to recognition performance.

2 Related works

2.1 Plankton recognition

As automated plankton imaging instruments now enable large-scale and even real-time monitoring of plankton communities, efficient automatic recognition

methods are essential. Existing approaches range from early feature-engineering methods [30] to modern deep learning models [8]. Current state-of-the-art techniques typically employ either Convolutional Neural Networks (CNNs) [22] or transformer-based architectures such as Vision Transformers (ViTs) [23], often combined with self-supervised or transfer learning strategies [17,23,26]. Research on plankton recognition has mainly focused on developing models for image data, with studies related to recognition of the pulse shape profiles being scarce [13]

Most existing work on plankton recognition has focused on developing models for one or a few specific datasets using labeled training sets. Consequently, numerous models have been proposed that perform well on a single imaging instrument and a fixed set of species but fail to generalize to other datasets. Creating new manually annotated image datasets for instrument deployments in new locations with varying species composition is impractical, highlighting the need for more generalizable methods. Recent efforts have addressed this shortcoming through open-set recognition [1, 18, 36] and domain adaptation [2, 5]. However, developing robust and generalizable models that minimize manual expert labeling remains essential for real-world plankton monitoring.

2.2 Multimodal learning

Multimodal machine learning utilizes a range of methods to jointly process and integrate information from multiple data sources, or modalities, (e.g., images, text, audio, sensor data) to produce context-aware representations for tasks like visual question answering and cross-modal retrieval [24]. A common approach is representation coordination, which aligns modality-specific representations in a shared embedding space to enforce semantic consistency across modalities while preserving their individual characteristics. This is typically achieved by using separate encoders for each modality and applying alignment constraints only at the embedding level [24].

Contrastive learning has become the dominant paradigm for representation coordination, starting from image–sentence alignment [20] and culminating in large-scale models such as CLIP [29]. These models maximize similarity between matching pairs (e.g., an image and its caption) and minimize it for non-matching pairs, enabling strong zero-shot generalization. Subsequent models, including Sigmoid loss for Language-Image Pre-training (SigLIP) [37] and SigLIP 2 [34], further improved optimization and scalability. Beyond vision–language, similar principles extend to other modality pairs, such as audio–text in Contrastive Language-Audio Pre-training (CLAP) [9], demonstrating the versatility of contrastive multimodal learning.

In the biological domain, BioCLIP [31] and BioCLIP 2 [15] adapt the CLIP framework for biological imaging tasks. Trained on millions of organism images paired with taxonomic labels, these models enable zero-shot classification across diverse biological datasets. Despite its success in broader biological contexts, BioCLIPs have shown limited effectiveness in direct plankton recognition [15,31].

Although multimodal learning has not been widely studied in plankton recognition, some studies have combined image data with supplementary metadata.

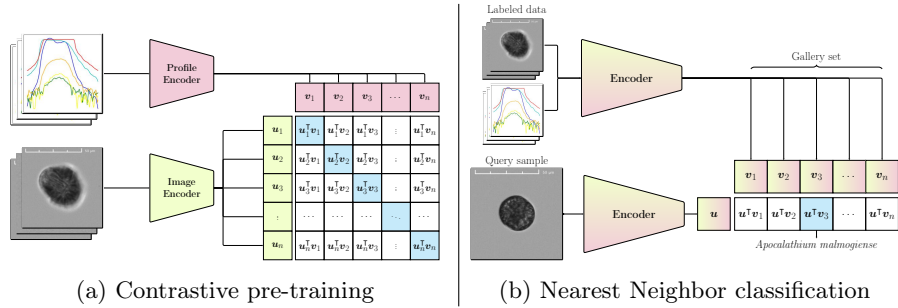


Fig. 2: Overview of the proposed multimodal recognition framework. (a) During pre-training, paired image–profile samples are aligned in a shared embedding space. (b) At inference, classification is performed using nearest-neighbor search in the embedding space.

These works typically use simple fusion strategies such as feature or input concatenation rather than coordinated representations. For example, Ellen *et al.* [10] combined image features with geotemporal and hydrographic metadata and Bures *et al.* [3] incorporated image size and geotemporal metadata. These works represent initial attempts to leverage multimodal information for plankton recognition, although they rely solely on metadata rather than true multi-sensor modalities, which is the focus of this study.

3 Methods

The proposed method adapts contrastive multimodal learning to plankton recognition. The pipeline consists of two stages: (1) contrastive pre-training to learn a shared multimodal embedding space, and (2) metric-based classification using nearest neighbors. The overall methodology is illustrated in Fig. 2.

3.1 Contrastive Image–Profile Pre-training

The pre-training stage adapts the contrastive learning framework of CLIP [29] by aligning plankton images with their corresponding optical profiles rather than text. In this setup, each image–profile pair represents a single plankton particle, and the model learns a shared embedding space where paired samples are close and unpaired samples are far apart. Unlike CLIP, which leverages language to structure embeddings for open-vocabulary tasks, our approach uses physical measurements to capture domain-specific properties of plankton data.

Formally, let $\mathcal{B} := \{(\mathbf{x}_i, \mathbf{x}_p)\}_{i=1}^n$ be a batch of n multimodal samples, where \mathbf{x}_i is an image and \mathbf{x}_p the corresponding profile. Two modality-specific encoders, f_i and f_p , produce intermediate representations:

$$\mathbf{r}_i = f_i(\mathbf{x}_i), \quad \mathbf{r}_p = f_p(\mathbf{x}_p),$$

where $\mathbf{r}_i \in \mathbb{R}^u$ and $\mathbf{r}_p \in \mathbb{R}^v$. These representations are projected into a shared d -dimensional space via linear layers L_i and L_p :

$$\mathbf{e}_i = L_i(\mathbf{r}_i), \quad \mathbf{e}_p = L_p(\mathbf{r}_p), \quad \mathbf{e}_i, \mathbf{e}_p \in \mathbb{R}^d.$$

After ℓ_2 normalization, similarity between two embeddings is measured using cosine similarity:

$$S(\mathbf{e}_i, \mathbf{e}_p) = \frac{\mathbf{e}_i^\top \mathbf{e}_p}{\|\mathbf{e}_i\| \|\mathbf{e}_p\|}.$$

InfoNCE loss. We adopt the InfoNCE contrastive loss [27], which has been widely used in multimodal representation learning. The loss encourages matched image–profile pairs to have higher similarity than mismatched pairs in the embedding space. The loss is computed using symmetric cross-entropy loss for both modalities. For image-to-profile alignment:

$$\mathcal{L}_{i \rightarrow p} = -\frac{1}{n} \sum_{k=1}^n \log \frac{\exp(\tau S(\mathbf{e}_i^k, \mathbf{e}_p^k))}{\sum_{j=1}^n \exp(\tau S(\mathbf{e}_i^k, \mathbf{e}_p^j))},$$

where τ is a learnable temperature parameter. The profile-to-image alignment loss $\mathcal{L}_{p \rightarrow i}$ is computed in the same way, and the final loss is the average of the two.

Sigmoid loss. Additionally, we adopt the sigmoid loss introduced in SigLIP [37], which replaces the softmax normalization with independent binary classification for all pairs. The objective is a sigmoid-based binary cross-entropy:

$$\mathcal{L}_{\text{Sigmoid}} = -\frac{1}{n} \sum_{i=1}^n \sum_{j=1}^n \log \frac{1}{1 + \exp(-z_{i,j}(\tau S(\mathbf{e}_i, \mathbf{e}_p) + b))},$$

where $z_{i,j} = 1$ when $i = j$ (positive pair), and -1 otherwise. Here τ is a learnable temperature parameter, and b is a learnable bias term that improves stability during early training.

3.2 Nearest Neighbor classification

After pre-training, the learned multimodal embedding space is reused for classification. In contrast to the original CLIP, which compares image embeddings against a fixed set of text embeddings, here we construct a gallery of labeled multimodal embeddings.

Formally, a gallery set is generated by encoding labeled plankton samples from all classes and modalities with the pretrained encoders. Each gallery embedding serves as a reference to a known class. Given a new test sample \mathbf{v} , its embeddings are compared to the gallery embeddings \mathbf{u}_i using cosine distance

$$D(\mathbf{u}_i, \mathbf{v}) = 1 - S(\mathbf{u}_i, \mathbf{v}),$$

and classification is based on the nearest neighbors. To improve robustness, k -nearest neighbor voting is used instead of a single nearest neighbor.

The framework naturally supports multimodal test samples. Each modality is encoded separately, and k neighbors are retrieved for each embedding. The neighbors are then combined, and the final prediction is done based on the majority vote. Compared to the text-based lookup in CLIP, this design places no restrictions on the number of reference samples per class, and benefits directly from a larger gallery set.

4 Experiments

4.1 Data

Three multimodal plankton datasets acquired with the CytoSense (CS) instrument are utilized [7, 14]. CytoSense is a flow cytometer designed for multimodal plankton analysis. The device provides optical profiles for each particle with a complementary set of bright-field images. For this study, we used a dataset with each sample (data point pair) consisting of both:

1. **Bright-field image:** a gray-scaled image, analyzed on a size range of 0.5–800 μm , covering most phytoplankton particles.
2. **Optical profile:** a set of six optical signals measured as each particle passes through the laser. Signals are excited by a blue (488 nm) and an orange laser (596 nm) and detected by sensors for Forward Scatter (FSC), Sideward Scatter (SSC), and fluorescence in the green (502–538 nm), yellow (553–577 nm), orange (604–644 nm), and red (668–726 nm) channels.

The six optical signals can be represented as a sequence of T optical feature vectors

$$\mathbf{P} = [\mathbf{p}_1 \dots \mathbf{p}_T], \quad \mathbf{p}_t = \begin{bmatrix} \text{FSC}(t) \\ \text{SSC}(t) \\ \text{Green}(t) \\ \text{Yellow}(t) \\ \text{Orange}(t) \\ \text{Red}(t) \end{bmatrix},$$

where t denotes the position along the particle. In the image $\mathbf{I} \in \mathbb{R}^{H \times W}$, the length axis of the plankton is oriented horizontally. Example image–profile pairs are shown in Fig. 3.

In total, we utilize three multimodal datasets, namely the LAB, SEA, and UTO datasets, and publish them as a collection under SYKE-Plankton_CytoSense_2025 [19]. Two datasets are labeled and one unlabeled. An overview of the datasets is presented in Table 1.

The **LAB** dataset consists of 20,050 samples from 24 monospecific phytoplankton cultures obtained from the FINMARI Culture Collection of Syke Marine Research Laboratory and Tvärminne Zoological Station in March 2022. The dataset shares the same source material as DAPlankton_{LAB} [2] but includes a

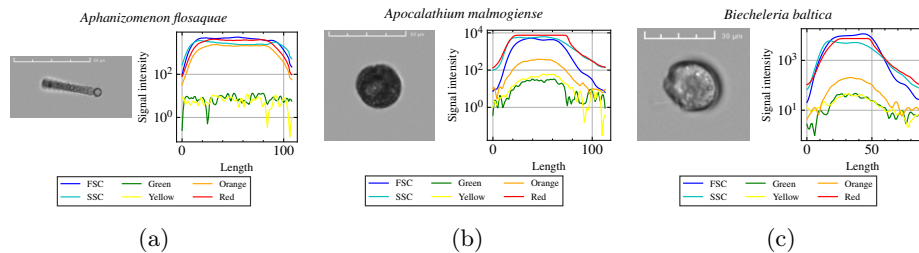


Fig. 3: Example image and profile data

Table 1: Summary of the datasets used in the experiments.

Dataset	Instrument	Number of classes	Samples per class	Total
LAB	CS-2019-97	24	543 – 1,285	20,050
SEA	CS-2019-97	38	1 – 2,594	9,353
UTO	CS-2021-103	unknown	unknown	32,930

larger set of classes, as it is not restricted to species present across multiple imaging instruments.

The **SEA** dataset consists of 9,353 samples across 38 classes collected *in situ* in the Baltic Sea in July 2020. Similarly to the **LAB** dataset, it shares the source material with DAPlankton_{SEA} [2]. The dataset is heavily imbalanced, with the largest class accounting for over 25% of all samples. Compared to DAPlankton_{SEA}, the SEA dataset includes additional classes but fewer total samples, as some images were missing the profile information.

The **UTO** dataset consists of 32,930 CytoSense samples collected *in situ* in the Baltic Sea between March 2024 and October 2024. The instrument was sampling hourly in an automated mode from the flow through system at the Utö Marine and Atmospheric Research Station (for details see [21]). The dataset contains raw, unfiltered data used exclusively for self-supervised pre-training.

4.2 Data pre-processing and augmentation

Preprocessing and augmentation were designed to maintain cross-modal consistency between images and optical profiles. For images, the scale bar was cropped, the remaining region padded to a square using edge padding to preserve aspect ratio, and the square resized to 236×236 pixels. Images were converted to grayscale and randomly cropped to 224×224 with a scale sampled from $(0.8, 1.0)$. Random vertical flips and color jitter, altering brightness and contrast within $(0.8, 1.2)$, were applied, followed by normalization to the range $(-1, 1)$.

For optical profiles, each signal was resampled to a fixed length of 224, transformed with logarithmic compression $\log(1 + x)$ to reduce magnitude variation while preserving relative shape, and normalized to $(-1, 1)$. Two stochastic augmentations were applied: random amplitude scaling, which perturbs the optical

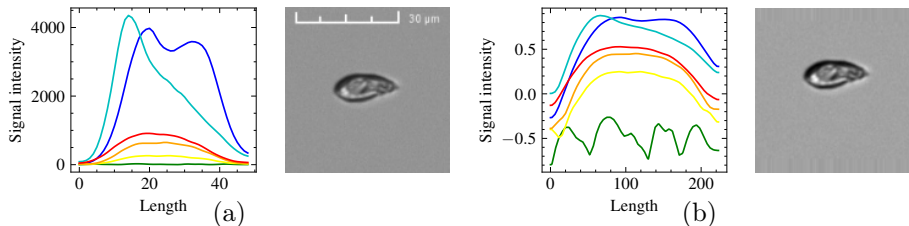


Fig. 4: Pre-processing and data augmentations: (a) original profile and image, (b) same pair pre-processed

signal intensity, and random band dropping, which zeroes out some of the signals. Finally, random horizontal flipping was applied synchronously to both modalities. An example of original and pre-processed samples is shown in Fig. 4.

4.3 Experimental Setup

We systematically evaluated our proposed pre-training strategy by combining different image encoders, profile encoders, and loss functions to assess in-domain and cross-domain performance. The goal was to determine how architectural and loss-function choices influence multimodal representation quality. Specifically, we compared three image encoders: EfficientNet B0 [33], ConvNeXt Femto [25], and ViT-Tiny [6], representing convolutional, modern convolutional, and transformer-based architectures, respectively. These variants were chosen to maintain similar model sizes because our training datasets were relatively small, making lightweight architectures more suitable (5 – 7M parameters). For the optical profile modality, we evaluated three sequence encoders: 1D CNN, bidirectional Long Short-Term Memory (LSTM) [16], and Transformer [35]. Lastly, two contrastive loss formulations were tested: InfoNCE [27] and Sigmoid loss [37].

In addition to the learned representations from each encoder, we appended the original image size (prior to cropping and padding) and the raw scattering profile length (prior to resampling) to the respective modality feature vectors before the projection heads. These scalar features were divided by the final target size (224), producing normalized values that encode the relative scale of each sample with respect to the resized input.

All models were trained using Stochastic Gradient Descent (SGD) with Nesterov momentum [32] of 0.9 and weight decay of 0.001. The learning rate was set to 0.005 for InfoNCE and 0.002 for Sigmoid loss and scheduled using a cosine annealing with 5 epoch linear warm up. Training was performed for up to 100 epochs, unless otherwise stated, using a batch size of 256, with early stopping applied if the validation loss did not improve for 30 consecutive epochs. 512 was used as the common embedding space dimension.

Throughout the experiments, we use the notation: [training set] \rightarrow [test set]. For example, LAB \rightarrow SEA indicates that the model was trained on the LAB dataset and tested on SEA. We use similar notation to denote modalities in the

gallery and query sets (e.g., I+P \rightarrow I means the gallery contains both modalities, while the query set contains only images). In all results, we used a gallery set of 16 samples, k -NN k value of 3, and randomly resampled the gallery set 10 times to mitigate sampling bias.

4.4 Results

In-domain Evaluation. The first experiment, evaluated in-domain performance on the LAB dataset using 5-fold cross-validation with stratified splits: 80% training, 5% validation, and 15% testing. Table 2 presents the average accuracies and standard deviations for different encoder combinations and loss functions. Notably, the InfoNCE loss consistently outperforms the Sigmoid loss across all configurations, indicating its superior ability to align image and optical profile modalities in a shared embedding space, especially in this low-data regime. Of the profile encoders, CNN achieved the highest accuracy, followed by Transformer and LSTM. In the later experiments, we focused the evaluation on the CNN and Transformer profile encoders and exclusively used InfoNCE loss, as LSTM and the Sigmoid loss consistently yielded lower performance.

Table 3 provides the complete breakdown for the best-performing configuration identified above: ViT-Tiny as the image encoder, CNN as the profile encoder, and InfoNCE as the loss function. The highest accuracy was achieved when both images and profiles are present in both the gallery and test sets (I+P \rightarrow I+P), confirming the benefit of multimodal recognition. Additionally, using only profiles in the gallery set yields better performance than using only images. This advantage is, however, largely due to the LAB dataset containing species with distinct optical characteristics. Somewhat surprisingly, recognition accuracy remains high even when the gallery and test sets use different modalities (e.g., I \rightarrow P), suggesting effective modality alignment. The full results for all configurations are presented in the supplementary material.

Cross-domain Evaluation. Table 4 presents the cross-domain performance of the image and optical profile encoder pairs trained with the InfoNCE loss. The most notable trend is that models pretrained on the UTO dataset generalize better to SEA than those trained on LAB. This result suggests that the

Table 2: In-domain average accuracy and standard deviation (%) for LAB \rightarrow LAB with I+P \rightarrow I+P

Loss	Model	CNN	LSTM	Transformer
InfoNCE	EfficientNet B0	95.06 \pm 0.58	89.59 \pm 0.67	92.11 \pm 0.98
	ConvNeXt Femto	94.81 \pm 0.90	90.10 \pm 0.67	89.85 \pm 3.84
	ViT Tiny	96.01 \pm0.56	90.39 \pm 0.66	91.80 \pm 0.76
Sigmoid	EfficientNet B0	91.85 \pm 0.65	84.13 \pm 0.77	85.98 \pm 1.28
	ConvNeXt Femto	89.93 \pm 1.81	85.82 \pm 1.50	86.56 \pm 2.54
	ViT Tiny	94.89 \pm 0.43	87.45 \pm 1.15	90.24 \pm 1.27

Table 3: Average accuracy and standard deviation for the best configuration (ViT-Tiny, CNN, InfoNCE) on LAB \rightarrow LAB

Gallery Test	I	P	I+P
I	92.73 \pm 0.59	93.03 \pm 0.69	94.24 \pm 0.59
P	91.56 \pm 0.67	94.51 \pm 0.83	95.42 \pm 0.73
I+P	92.79 \pm 0.57	94.55 \pm 0.82	96.01 \pm0.56

Table 4: Cross-domain average accuracy and standard deviation (%) for different image and profile encoder combinations with I+P \rightarrow I+P

Model	LAB \rightarrow SEA		UTO \rightarrow LAB		UTO \rightarrow SEA	
	CNN	Transf.	CNN	Transf.	CNN	Transf.
EfficientNet B0	67.57 \pm 2.23	66.87 \pm 2.07	84.22 \pm 0.99	88.35 \pm0.70	72.86 \pm1.85	69.04 \pm 2.01
ConvNeXt Femto	68.05 \pm2.06	64.49 \pm 3.42	83.73 \pm 0.79	88.13 \pm 0.74	70.63 \pm 1.77	68.90 \pm 2.27
ViT Tiny	66.75 \pm 2.21	66.42 \pm 1.90	86.81 \pm 0.83	88.30 \pm 0.71	71.75 \pm 1.48	69.14 \pm 1.75

stable growing conditions of the cultures used in the LAB dataset yield less variability (e.g., due to physiology and diversity), thus representing only a fraction of the heterogeneity found in the wild, and limiting the generalization of the LAB dataset to real-world plankton distributions. In contrast, the results for the UTO dataset demonstrates that unlabeled data can produce strong multimodal embeddings without manual annotations. As regards architectural choices, differences between the image encoders remain small, while for profile encoding CNN tends to outperform Transformer when applied to the SEA dataset.

Combined Training. Table 5 shows the performance obtained by training the encoders with LAB and UTO datasets and evaluating them on the SEA dataset, including results for both the original model sizes and their larger variants (18-28 M parameters): EfficientNet-B4, ConvNeXt-Tiny, and ViT-Small. Larger models were included to assess whether increased capacity improves performance when the amount of training data is larger. For larger models, the profile encoders were also scaled to keep the relative size of the encoders same. The results indicate that the CNN-based profile encoder performs worse than UTO-only training, whereas the Transformer-based encoder shows improvement. For larger models, we observe the opposite trend, suggesting that the available training data may be insufficient for the larger Transformer-based profile encoder.

Effect of Gallery Set Size. To analyze the impact of gallery set size on recognition accuracy, we evaluated the two best-performing image encoders (EfficientNet-B0 and ViT-Tiny) along with CNN- and Transformer-based profile encoders. Fig. 5 illustrates the mean accuracy and standard deviation as a function of gallery set size, with n being the number of multimodal samples per class. As

Table 5: Average accuracy and standard deviation (%) for combined training, UTO + LAB \rightarrow SEA with I+P \rightarrow I+P

Model	CNN	Transformer
EfficientNet B0	71.05 \pm 2.87	72.13 \pm 2.03
ConvNeXt Femto	71.77 \pm 2.42	71.67 \pm 1.53
ViT Tiny	71.37 \pm 2.17	72.73 \pm1.20
EfficientNet B4	74.94 \pm2.33	71.78 \pm 2.99
ConvNeXt Tiny	73.77 \pm 2.24	71.74 \pm 2.39
ViT Small	72.75 \pm 2.04	71.04 \pm 1.40

expected, accuracy improves steadily as the gallery size increases, confirming that larger reference sets improve embedding robustness. Additionally, models with CNN profile encoders perform worse with small gallery sets, but improve faster than transformers. The choice of image encoder architecture has only a minor effect on performance at this scale.

Comparison with Self-supervised Learning Baseline. We compared the performance of our multimodal model against an image-only self-supervised baseline DINO [4]. DINO was selected as it has been shown to produce strong visual representations directly through self-supervised training without requiring additional fine-tuning [4]. Detailed training configurations for all models are provided in the supplementary material.

Table 6 presents results across all domains and architectures. When evaluated using only image data (I \rightarrow I), the multimodal contrastive model consistently outperforms DINO, indicating that multimodal pre-training enhances the quality of visual representations even in unimodal settings. When both image and profile modalities are available during inference (I+P \rightarrow I+P), the multimodal model achieves further gains, demonstrating the effectiveness of joint multimodal embeddings for improving domain generalization and overall classification performance.

5 Conclusion

In this work, we explored the benefits of label-free cross-modal contrastive pre-training for plankton recognition. We introduced multimodal datasets and evaluated multiple image and profile encoder combinations and contrastive learning losses under in-domain and cross-domain settings. The results show that multimodal representation coordination significantly improves recognition accuracy compared to single-modality approaches, particularly when both modalities are available during inference.

Beyond improving recognition accuracy, we further demonstrated that pre-training on raw, unlabeled data from diverse environments enables cross-domain

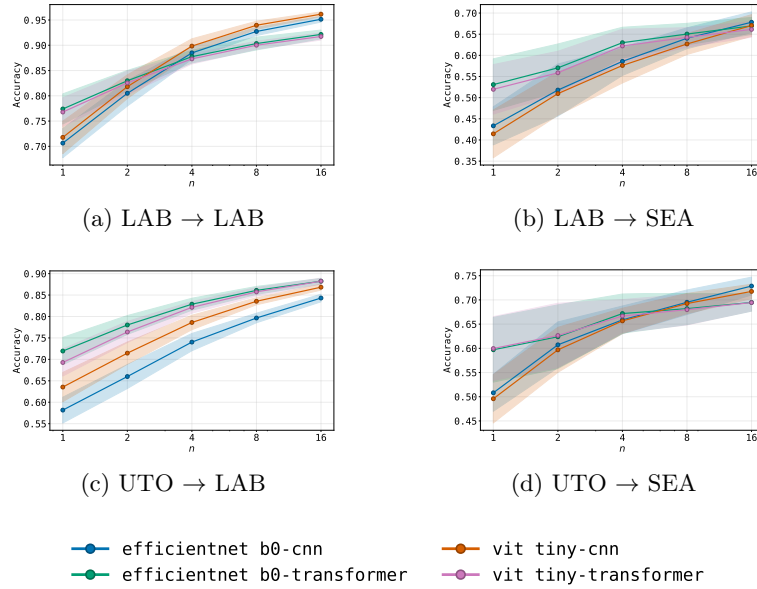


Fig. 5: Average accuracy and standard deviation as a function of gallery set size, with n being the number of multimodal samples in the gallery set ($I+P \rightarrow I+P$)

generalization, outperforming models trained on controlled laboratory data. This finding highlights the potential of leveraging raw *in-situ* data collected in real-world conditions to reduce reliance on manual annotation and improve scalability. To promote research in multimodal plankton recognition we have made our datasets publicly available [19].

Acknowledgments. The research was carried out in the FASTVISION and FASTVISION-plus projects funded by the Academy of Finland (Decision numbers 321980, 321991, 339612, and 339355).

Disclosure of Interests. The authors have no competing interests to declare that are relevant to the content of this article.

References

1. Badreldeen Bdwaw Mohamed, O., Eerola, T., Kraft, K., et al.: Open-set plankton recognition using similarity learning. In: ISVC (2022)
2. Batrakhanov, D., Eerola, T., Kraft, K., et al.: Daplankton: Benchmark dataset for multi-instrument plankton recognition via fine-grained domain adaptation. In: ICIP (2024)
3. Bureš, J., Eerola, T., Lensu, L., Kälviäinen, H., Zemčík, P.: Plankton recognition in images with varying size. In: ICPR (2021)

Table 6: Average accuracy and standard deviation (%) comparing DINO and contrastive multimodal pre-training

Method	Model	LAB → LAB	LAB → SEA	UTO → LAB	UTO → SEA
DINO	EfficientNet B0	79.67 ±1.42	57.30 ±2.29	57.24 ±0.81	63.19 ±2.29
	ConvNeXt Femto	62.85 ±2.82	55.52 ±3.29	54.76 ±0.87	55.58 ±1.75
	ViT Tiny	59.54 ±2.04	54.59 ±1.83	53.24 ±1.01	59.10 ±2.42
InfoNCE (I→I)	EfficientNet B0	91.62 ±1.05	66.04 ±1.60	69.87 ±1.21	72.56 ±1.98
	ConvNeXt Femto	90.01 ±0.98	65.62 ±1.88	66.03 ±1.13	72.05 ±1.84
	ViT Tiny	92.79 ±0.55	64.37 ±1.94	66.11 ±1.22	70.83 ±1.68
InfoNCE (I+P→I+P)	EfficientNet B0	95.06 ±0.58	67.57 ±2.23	88.35 ±0.70	72.86 ±1.85
	ConvNeXt Femto	94.81 ±0.90	68.05 ±2.06	88.13 ±0.74	70.63 ±1.77
	ViT Tiny	96.01 ±0.56	66.75 ±2.21	88.30 ±0.71	71.75 ±1.48

- Caron, M., Touvron, H., Misra, I., Jégou, H., Mairal, J., Bojanowski, P., Joulin, A.: Emerging properties in self-supervised vision transformers. In: CVPR (2021)
- Chen, C., Kyathanahally, S.P., Reyes, M., et al.: Producing plankton classifiers that are robust to dataset shift. *Limnology and Oceanography: Methods* **23**, 39–66 (2025)
- Dosovitskiy, A., Beyer, L., Kolesnikov, A., et al.: An image is worth 16x16 words: Transformers for image recognition at scale. In: ICLR (2021)
- Dubelaar, G.B., Gerritzen, P.L., Beeker, A.E., Jonker, R.R., Tangen, K.: Design and first results of cytobuoy: A wireless flow cytometer for in situ analysis of marine and fresh waters. *Cytometry* **37**, 247–254 (1999)
- Eerola, T., Batrakhonov, D., Barazandeh, N.V., et al.: Survey of automatic plankton image recognition: challenges, existing solutions and future perspectives. *Artificial Intelligence Review* **57** (2024)
- Elizalde, B., Deshmukh, S., Al Ismail, M., Wang, H.: Clap learning audio concepts from natural language supervision. In: ICASSP (2023)
- Ellen, J.S., Graff, C.A., Ohman, M.D.: Improving plankton image classification using context metadata. *Limnology and Oceanography: Methods* **17**, 439–461 (2019)
- Falkowski, P.G.: The role of phytoplankton photosynthesis in global biogeochemical cycles. *Photosynthesis research* **39**, 235–258 (1994)
- Field, C.B., Behrenfeld, M.J., Randerson, J.T., Falkowski, P.: Primary production of the biosphere: integrating terrestrial and oceanic components. *Science* **281**, 237–240 (1998)
- Fuchs, R., Thyssen, M., Creach, V., et al.: Automatic recognition of flow cytometric phytoplankton functional groups using convolutional neural networks. *Limnology and Oceanography: Methods* **20**(7), 387–399 (2022)
- Gallot, C., Hubert, Z., Haraguchi, L., et al.: Best practices for optimization of phytoplankton analysis in natural waters using cytosense flow cytometers. *Cytometry Part A* (2025)
- Gu, J., Stevens, S., Campolongo, E.G., et al.: Bioclip 2: Emergent properties from scaling hierarchical contrastive learning (2025), <https://arxiv.org/abs/2505.23883>
- Hochreiter, S., Schmidhuber, J.: Long short-term memory. *Neural Computation* **9**, 1735–1780 (1997)
- Kareinen, J., Eerola, T., Kraft, K., Lensu, L., Suikkanen, S., Kälviäinen, H.: Self-supervised pretraining for fine-grained plankton recognition. In: CVPR Workshops (2025)

18. Kareinen, J., Skyttä, A., Eerola, T., et al.: Open-set plankton recognition. In: ECCV Workshops (2024)
19. Kareinen, J., Veikka, I., Eerola, T., Haraguchi, L., Lensu, L., Kraft, K., Suikkanen, S., Kälviäinen, H.: SYKE-plankton_CytoSense_2025. <https://ida.fairdata.fi/s/NOT-FOR-PUBLICATION-HcirdqiwoMzb> (2025)
20. Kiros, R., Salakhutdinov, R., Zemel, R.S.: Unifying visual-semantic embeddings with multimodal neural language models (2014), <https://arxiv.org/abs/1411.2539>
21. Kraft, K., Haraguchi, L., Hällfors, H., et al.: Monitoring cyanobacteria blooms with complementary measurements—a similar story told using high-throughput imaging, optical sensors, light microscopy, and satellite-based methods. *Harmful Algae* p. 102865 (2025)
22. Kraft, K., Velhonoja, O., Seppälä, J., et al.: SYKE-plankton_IFCB_2022 (2022). <https://doi.org/10.23728/b2share.abf913e5a6ad47e6baa273ae0ed6617a>
23. Kyathanahally, S., Hardeman, T., Reyes, M., Merz, E., Bulas, T., Brun, P., Pomati, F., Baity-Jesi, M.: Ensembles of data-efficient vision transformers as a new paradigm automated classification in ecology. *Scientific Reports* **12**, 18590 (2022)
24. Liang, P.P., Zadeh, A., Morency, L.P.: Foundations & trends in multimodal machine learning: Principles, challenges, and open questions. *ACM Computing Surveys* **56**, 1–42 (2024)
25. Liu, Z., Mao, H., Wu, C.Y., Feichtenhofer, C., Darrell, T., Xie, S.: A convnet for the 2020s. In: CVPR (2022)
26. Maracani, A., Pastore, V.P., Natale, L., Rosasco, L., Odone, F.: In-domain versus out-of-domain transfer learning in plankton image classification. *Scientific Reports* **13**, 10443 (2023)
27. van den Oord, A., Li, Y., Vinyals, O.: Representation learning with contrastive predictive coding (2018), <https://arxiv.org/abs/1807.03748>
28. Orenstein, E.C., Beijbom, O., Peacock, E.E., Sosik, H.M.: WHOI-Plankton- A Large Scale Fine Grained Visual Recognition Benchmark Dataset for Plankton Classification (2015), <https://arxiv.org/abs/1510.00745>
29. Radford, A., Kim, J.W., Hallacy, C., et al.: Learning transferable visual models from natural language supervision. In: ICML (2021)
30. Sosik, H.M., Olson, R.J.: Automated taxonomic classification of phytoplankton sampled with imaging-in-flow cytometry. *Limnology and Oceanography: Methods* **5**, 204–216 (2007)
31. Stevens, S., Wu, J., Thompson, M.J., et al.: Bioclip: A vision foundation model for the tree of life. In: CVPR (2024)
32. Sutskever, I., Martens, J., Dahl, G., Hinton, G.: On the importance of initialization and momentum in deep learning. In: ICML (2013)
33. Tan, M., Le, Q.: EfficientNet: Rethinking model scaling for convolutional neural networks. In: ICML (2019)
34. Tschannen, M., Gritsenko, A., Wang, X., et al.: Siglip 2: Multilingual vision-language encoders with improved semantic understanding, localization, and dense features (2025), <https://arxiv.org/abs/2502.14786>
35. Vaswani, A., Shazeer, N., Parmar, N., et al.: Attention is all you need. In: NeurIPS (2017)
36. Yang, Z., Li, J., Chen, T., Pu, Y., Feng, Z.: Contrastive learning-based image retrieval for automatic recognition of in situ marine plankton images. *ICES Journal of Marine Science* pp. 2643–2655 (2022)
37. Zhai, X., Mustafa, B., Kolesnikov, A., Beyer, L.: Sigmoid loss for language image pre-training. In: CVPR (2023)

Appendix

A.1. Profile encoder architectures

The design choices for each encoder were made to balance representational capacity and computational efficiency, given the relatively small dataset size. Detailed configuration parameters for each model are provided below.

CNN. The CNN-based encoder follows the ResNet18 design with the key modification of using only 1D convolutions. The main parameters are summarized in Table 7:

Table 7: Configuration of the 1D CNN encoder.

Parameter	Value
Input size	6
Output size	257
Blocks	[2, 2, 2, 2]
Base channels	32
Dropout	0.2
Params	963K

Bidirectional LSTM. The Bidirectional LSTM captures sequential dependencies in both the forward and backward directions. During our experimentation we found that using a single-layer LSTM was sufficient, as adding more layers did not improve performance. The encoder configuration is listed in Table 8.

Table 8: Configuration of the Bidirectional LSTM encoder.

Parameter	Value
Input size	6
Output size	257
Hidden size	128
N layers	1
Dropout	0.2
Params	264K

Transformer. The Transformer encoder adopted a lightweight configuration inspired by ViT-Tiny, consisting of six encoder layers with four attention heads per layer and GELU activations in the feedforward layers. Table 9 summarizes the parameters.

Table 9: Configuration of the Transformer encoder.

Parameter	Value
Input size	6
Output size	129
Hidden size	128
N heads	4
N layers	6
Feedforward Dim	256
Dropout	0.2
Params	1.1M

A.2. In-domain Evaluation Full Results

The full results for the in-domain evaluation with all encoder pairs with InfoNCE loss can be seen in Table 10 and for Sigmoid loss in Table 11. Notably, InfoNCE does better in all cases. When comparing LSTM to the other two encoders, the results show that especially in $I \rightarrow P$ and $P \rightarrow I$, LSTM attains much lower accuracy.

A.3. Cross-domain Evaluation Full Results

Full results for the cross-domain evaluation, using all image encoders and the CNN/Transformer profile encoder with InfoNCE loss are presented in Tables 12, 13, 14 for $LAB \rightarrow SEA$, $UTO \rightarrow LAB$, and $UTO \rightarrow SEA$ respectively. Notably, in the cross-domain setting, the cross-modal performance ($I \rightarrow P$, $P \rightarrow I$) is significantly worse than the intramodal performance ($I \rightarrow I$, $P \rightarrow P$). This result seems to indicate that with more realistic profile data the model does not actually manage to coordinate the representations, possibly due to the low amount of training data used or the long-tailed nature of the data. However, despite the low cross-modal performance, the model achieves very high accuracy when the modalities are used either independently or combined.

A.4. Combined Training Full Results.

Full results for the combined training are presented in Tables 15, and 16 for the smaller and larger model variants respectively. For the larger profile encoders we increased the base channels from 32 to 64 for CNN, and hidden dimension from 128 to 256 and feedforward dimension from 256 to 512 for transformer. The resulting sizes in parameters were 3.8M and 3.7M for CNN and transformer respectively.

Table 10: Full results, LAB \rightarrow LAB, InfoNCE

EfficientNet B0 + CNN			ConvNeXt Femto + CNN			ViT-Tiny + CNN		
Gallery	Test	Accuracy	Gallery	Test	Accuracy	Gallery	Test	Accuracy
I	I	89.76±0.65%	I	I	89.21±2.57%	I	I	92.73±0.59%
I	P	90.95±0.80%	I	P	91.27±1.19%	I	P	93.03±0.69%
I	I+P	92.01±0.68%	I	I+P	91.68±1.96%	I	I+P	94.24±0.59%
P	I	89.05±0.83%	P	I	89.09±1.99%	P	I	91.56±0.67%
P	P	93.93±0.69%	P	P	93.73±0.68%	P	P	94.51±0.83%
P	I+P	94.65±0.68%	P	I+P	94.41±0.78%	P	I+P	95.42±0.73%
I+P	I	89.82±0.64%	I+P	I	89.26±2.58%	I+P	I	92.79±0.57%
I+P	P	93.97±0.71%	I+P	P	93.76±0.66%	I+P	P	94.55±0.82%
I+P	I+P	95.06±0.58%	I+P	I+P	94.81±0.90%	I+P	I+P	96.01±0.56%
EfficientNet B0 + LSTM			ConvNeXt Femto + LSTM			ViT-Tiny + LSTM		
Gallery	Test	Accuracy	Gallery	Test	Accuracy	Gallery	Test	Accuracy
I	I	89.78±0.71%	I	I	90.01±0.98%	I	I	90.95±0.67%
I	P	76.62±1.43%	I	P	78.46±1.00%	I	P	78.76±1.44%
I	I+P	90.76±0.73%	I	I+P	90.92±0.85%	I	I+P	91.64±0.63%
P	I	80.23±1.11%	P	I	81.20±1.17%	P	I	82.11±0.93%
P	P	82.60±0.90%	P	P	81.84±0.86%	P	P	81.64±0.87%
P	I+P	83.95±0.81%	P	I+P	83.59±0.80%	P	I+P	83.39±0.81%
I+P	I	89.75±0.71%	I+P	I	90.01±0.99%	I+P	I	90.95±0.67%
I+P	P	82.60±0.90%	I+P	P	81.84±0.85%	I+P	P	81.65±0.87%
I+P	I+P	89.59±0.67%	I+P	I+P	90.10±0.67%	I+P	I+P	90.39±0.66%
EfficientNet B0 + Transformer			ConvNeXt Femto + Transformer			ViT-Tiny + Transformer		
Gallery	Test	Accuracy	Gallery	Test	Accuracy	Gallery	Test	Accuracy
I	I	91.62±1.05%	I	I	88.67±6.48%	I	I	92.79±0.55%
I	P	86.64±1.70%	I	P	79.97±8.21%	I	P	85.36±1.24%
I	I+P	92.61±0.98%	I	I+P	89.72±6.21%	I	I+P	93.33±0.54%
P	I	87.41±1.03%	P	I	82.13±10.0%	P	I	87.58±1.18%
P	P	88.94±0.97%	P	P	86.28±3.60%	P	P	87.71±0.84%
P	I+P	89.60±1.04%	P	I+P	86.84±3.75%	P	I+P	88.37±0.82%
I+P	I	91.64±1.05%	I+P	I	88.67±6.48%	I+P	I	92.79±0.55%
I+P	P	88.94±0.97%	I+P	P	86.28±3.60%	I+P	P	87.71±0.84%
I+P	I+P	92.11±0.98%	I+P	I+P	89.85±3.84%	I+P	I+P	91.80±0.76%

A.5. Self-supervised Learning Baseline Configuration.

The image-only baseline DINO model was trained for 300 epochs using the adamW optimizer with a batch size of 512. The learning rate is linearly ramped up during the first 10 epochs to its base value, which was set to 0.005 for EfficientNet and 0.0001 for ConvNeXt and ViT. The learning rate was set lower for ConvNeXt and ViT as otherwise the models did not start learning. Following the original implementation, the weight decay follows a cosine decay from 0.04 to 0.4. The student temperature was set to 0.1 and the teacher temperature uses linear warm-up from 0.04 to 0.07 during the first 30 epochs.

For data augmentations, the scale bar was cropped, the remaining region padded to a square using edge padding to preserve aspect ratio, resized to 236×236 pixels, and converted to grayscale. Following this, we used the same augmentations that were used in the original implementation. 2 global and 6 local crops were used, with the local crop scale selected from (0.1, 0.4). For the

Table 11: Full results, LAB \rightarrow LAB, Sigmoid

EfficientNet B0 + CNN			ConvNeXt Femto + CNN			ViT-Tiny + CNN		
Gallery	Test	Accuracy	Gallery	Test	Accuracy	Gallery	Test	Accuracy
I	I	80.58 \pm 1.32%	I	I	75.25 \pm 3.76%	I	I	90.51 \pm 0.73%
I	P	84.41 \pm 1.37%	I	P	80.74 \pm 3.66%	I	P	91.32 \pm 0.87%
I	I+P	83.52 \pm 1.29%	I	I+P	77.43 \pm 3.83%	I	I+P	91.67 \pm 0.64%
P	I	79.55 \pm 1.20%	P	I	73.26 \pm 4.25%	P	I	88.97 \pm 0.77%
P	P	90.79 \pm 0.63%	P	P	89.46 \pm 1.68%	P	P	93.35 \pm 0.54%
P	I+P	91.10 \pm 0.64%	P	I+P	89.67 \pm 1.65%	P	I+P	93.68 \pm 0.56%
I+P	I	80.58 \pm 1.32%	I+P	I	75.25 \pm 3.76%	I+P	I	90.51 \pm 0.73%
I+P	P	90.79 \pm 0.63%	I+P	P	89.46 \pm 1.68%	I+P	P	93.35 \pm 0.54%
I+P	I+P	91.85 \pm 0.65%	I+P	I+P	89.93 \pm 1.81%	I+P	I+P	94.89 \pm 0.43%
EfficientNet B0 + LSTM			ConvNeXt Femto + LSTM			ViT-Tiny + LSTM		
Gallery	Test	Accuracy	Gallery	Test	Accuracy	Gallery	Test	Accuracy
I	I	82.11 \pm 0.93%	I	I	84.14 \pm 3.93%	I	I	87.93 \pm 1.53%
I	P	60.38 \pm 1.43%	I	P	63.33 \pm 2.56%	I	P	64.56 \pm 1.78%
I	I+P	83.75 \pm 0.80%	I	I+P	85.43 \pm 3.47%	I	I+P	88.69 \pm 1.36%
P	I	63.22 \pm 1.73%	P	I	65.39 \pm 5.04%	P	I	69.35 \pm 2.17%
P	P	75.23 \pm 1.11%	P	P	74.81 \pm 1.03%	P	P	74.63 \pm 1.19%
P	I+P	76.74 \pm 1.02%	P	I+P	76.66 \pm 1.02%	P	I+P	76.45 \pm 1.13%
I+P	I	82.10 \pm 0.93%	I+P	I	84.14 \pm 3.93%	I+P	I	87.93 \pm 1.53%
I+P	P	75.22 \pm 1.11%	I+P	P	74.81 \pm 1.03%	I+P	P	74.63 \pm 1.19%
I+P	I+P	84.13 \pm 0.77%	I+P	I+P	85.82 \pm 1.50%	I+P	I+P	87.45 \pm 1.15%
EfficientNet B0 + Transformer			ConvNeXt Femto + Transformer			ViT-Tiny + Transformer		
Gallery	Test	Accuracy	Gallery	Test	Accuracy	Gallery	Test	Accuracy
I	I	81.54 \pm 0.93%	I	I	83.48 \pm 8.13%	I	I	90.42 \pm 0.80%
I	P	73.33 \pm 1.81%	I	P	75.13 \pm 6.19%	I	P	81.21 \pm 1.98%
I	I+P	83.47 \pm 0.94%	I	I+P	84.68 \pm 7.51%	I	I+P	91.04 \pm 0.83%
P	I	71.46 \pm 1.90%	P	I	73.02 \pm 9.00%	P	I	82.19 \pm 2.89%
P	P	84.04 \pm 1.44%	P	P	83.38 \pm 2.32%	P	P	86.41 \pm 1.91%
P	I+P	84.34 \pm 1.43%	P	I+P	83.70 \pm 2.36%	P	I+P	86.88 \pm 1.87%
I+P	I	81.55 \pm 0.93%	I+P	I	83.48 \pm 8.13%	I+P	I	90.42 \pm 0.80%
I+P	P	84.04 \pm 1.44%	I+P	P	83.38 \pm 2.32%	I+P	P	86.41 \pm 1.91%
I+P	I+P	85.98 \pm 1.28%	I+P	I+P	86.56 \pm 2.54%	I+P	I+P	90.24 \pm 1.27%

DINO head, a hidden dimension of 256 was used, a bottleneck dimension of 64, and an output dimension of 512.

Table 12: Full results, LAB \rightarrow SEA, InfoNCE

EfficientNet B0 + CNN			ConvNeXt Femto + CNN			ViT-Tiny + CNN		
Gallery	Test	Accuracy	Gallery	Test	Accuracy	Gallery	Test	Accuracy
I	I	63.47 \pm 2.47%	I	I	62.84 \pm 2.12%	I	I	60.59 \pm 2.15%
I	P	29.35 \pm 3.80%	I	P	30.64 \pm 3.96%	I	P	29.64 \pm 4.08%
I	I+P	64.25 \pm 2.72%	I	I+P	63.80 \pm 2.70%	I	I+P	61.63 \pm 2.68%
P	I	28.58 \pm 4.75%	P	I	28.99 \pm 3.87%	P	I	25.94 \pm 4.23%
P	P	60.31 \pm 2.21%	P	P	60.71 \pm 2.38%	P	P	59.59 \pm 2.07%
P	I+P	61.11 \pm 2.34%	P	I+P	61.49 \pm 2.46%	P	I+P	60.19 \pm 2.09%
I+P	I	63.39 \pm 2.48%	I+P	I	62.76 \pm 2.12%	I+P	I	60.57 \pm 2.15%
I+P	P	60.33 \pm 2.20%	I+P	P	60.72 \pm 2.37%	I+P	P	59.61 \pm 2.06%
I+P	I+P	67.57 \pm 2.23%	I+P	I+P	68.05 \pm 2.06%	I+P	I+P	66.75 \pm 2.21%
EfficientNet B0 + Transformer			ConvNeXt Femto + Transformer			ViT-Tiny + Transformer		
Gallery	Test	Accuracy	Gallery	Test	Accuracy	Gallery	Test	Accuracy
I	I	66.04 \pm 1.60%	I	I	65.62 \pm 1.88%	I	I	64.37 \pm 1.94%
I	P	24.80 \pm 4.79%	I	P	21.98 \pm 5.42%	I	P	25.41 \pm 5.45%
I	I+P	66.28 \pm 1.77%	I	I+P	65.71 \pm 1.87%	I	I+P	64.80 \pm 2.04%
P	I	17.66 \pm 4.12%	P	I	16.36 \pm 4.89%	P	I	17.98 \pm 3.03%
P	P	61.88 \pm 2.16%	P	P	59.71 \pm 3.26%	P	P	61.41 \pm 2.00%
P	I+P	62.01 \pm 2.19%	P	I+P	59.81 \pm 3.30%	P	I+P	61.53 \pm 2.00%
I+P	I	66.04 \pm 1.60%	I+P	I	65.60 \pm 1.89%	I+P	I	64.36 \pm 1.94%
I+P	P	61.88 \pm 2.16%	I+P	P	59.71 \pm 3.26%	I+P	P	61.41 \pm 2.00%
I+P	I+P	66.87 \pm 2.07%	I+P	I+P	64.49 \pm 3.42%	I+P	I+P	66.42 \pm 1.90%

Table 13: Full results, UTO \rightarrow LAB, InfoNCE

EfficientNet B0 + CNN			ConvNeXt Femto + CNN			ViT-Tiny + CNN		
Gallery	Test	Accuracy	Gallery	Test	Accuracy	Gallery	Test	Accuracy
I	I	69.87 \pm 1.21%	I	I	66.03 \pm 1.13%	I	I	66.11 \pm 1.22%
I	P	17.54 \pm 2.17%	I	P	16.26 \pm 2.11%	I	P	13.97 \pm 2.31%
I	I+P	69.81 \pm 1.21%	I	I+P	66.15 \pm 1.22%	I	I+P	65.93 \pm 1.22%
P	I	16.35 \pm 1.20%	P	I	17.09 \pm 1.06%	P	I	16.27 \pm 1.32%
P	P	80.01 \pm 0.95%	P	P	80.97 \pm 0.93%	P	P	84.30 \pm 0.90%
P	I+P	79.96 \pm 1.00%	P	I+P	80.98 \pm 0.96%	P	I+P	84.38 \pm 0.91%
I+P	I	69.85 \pm 1.21%	I+P	I	66.01 \pm 1.14%	I+P	I	66.10 \pm 1.22%
I+P	P	80.01 \pm 0.95%	I+P	P	80.96 \pm 0.92%	I+P	P	84.31 \pm 0.89%
I+P	I+P	84.22 \pm 0.99%	I+P	I+P	83.73 \pm 0.79%	I+P	I+P	86.81 \pm 0.83%
EfficientNet B0 + Transformer			ConvNeXt Femto + Transformer			ViT-Tiny + Transformer		
Gallery	Test	Accuracy	Gallery	Test	Accuracy	Gallery	Test	Accuracy
I	I	69.43 \pm 1.10%	I	I	66.06 \pm 0.94%	I	I	62.41 \pm 1.22%
I	P	15.96 \pm 2.96%	I	P	15.96 \pm 2.84%	I	P	16.88 \pm 2.68%
I	I+P	69.08 \pm 1.07%	I	I+P	65.59 \pm 0.97%	I	I+P	62.43 \pm 1.26%
P	I	18.32 \pm 0.78%	P	I	14.20 \pm 0.79%	P	I	15.03 \pm 0.71%
P	P	87.33 \pm 0.79%	P	P	87.02 \pm 0.72%	P	P	87.45 \pm 0.71%
P	I+P	87.36 \pm 0.79%	P	I+P	87.04 \pm 0.75%	P	I+P	87.46 \pm 0.71%
I+P	I	69.43 \pm 1.09%	I+P	I	66.06 \pm 0.94%	I+P	I	62.41 \pm 1.22%
I+P	P	87.33 \pm 0.79%	I+P	P	87.02 \pm 0.72%	I+P	P	87.45 \pm 0.71%
I+P	I+P	88.35 \pm 0.70%	I+P	I+P	88.13 \pm 0.74%	I+P	I+P	88.30 \pm 0.71%

Table 14: Full results, UTO \rightarrow SEA, InfoNCE

EfficientNet B0 + CNN			ConvNeXt Femto + CNN			ViT-Tiny + CNN		
Gallery	Test	Accuracy	Gallery	Test	Accuracy	Gallery	Test	Accuracy
I	I	71.04 \pm 2.01%	I	I	66.38 \pm 2.48%	I	I	70.83 \pm 1.68%
I	P	31.37 \pm 3.94%	I	P	23.32 \pm 3.72%	I	P	25.61 \pm 3.36%
I	I+P	71.69 \pm 2.14%	I	I+P	65.96 \pm 2.83%	I	I+P	70.91 \pm 1.70%
P	I	21.49 \pm 2.01%	P	I	22.94 \pm 3.82%	P	I	25.12 \pm 4.67%
P	P	64.73 \pm 2.15%	P	P	63.62 \pm 1.96%	P	P	62.52 \pm 2.25%
P	I+P	64.98 \pm 2.17%	P	I+P	63.54 \pm 2.03%	P	I+P	62.62 \pm 2.35%
I+P	I	70.77 \pm 2.02%	I+P	I	66.07 \pm 2.52%	I+P	I	70.79 \pm 1.70%
I+P	P	64.73 \pm 2.15%	I+P	P	63.62 \pm 1.96%	I+P	P	62.52 \pm 2.24%
I+P	I+P	72.86 \pm 1.85%	I+P	I+P	70.63 \pm 1.77%	I+P	I+P	71.75 \pm 1.48%
EfficientNet B0 + Transformer			ConvNeXt Femto + Transformer			ViT-Tiny + Transformer		
Gallery	Test	Accuracy	Gallery	Test	Accuracy	Gallery	Test	Accuracy
I	I	72.56 \pm 1.98%	I	I	72.05 \pm 1.84%	I	I	68.48 \pm 1.44%
I	P	38.77 \pm 7.68%	I	P	32.53 \pm 6.29%	I	P	31.14 \pm 4.47%
I	I+P	73.08 \pm 1.70%	I	I+P	72.65 \pm 1.61%	I	I+P	69.23 \pm 1.36%
P	I	23.43 \pm 3.21%	P	I	19.63 \pm 4.79%	P	I	21.54 \pm 3.28%
P	P	64.55 \pm 1.93%	P	P	64.12 \pm 2.38%	P	P	64.37 \pm 2.14%
P	I+P	64.64 \pm 1.93%	P	I+P	64.08 \pm 2.44%	P	I+P	64.36 \pm 2.13%
I+P	I	72.55 \pm 1.99%	I+P	I	72.05 \pm 1.85%	I+P	I	68.48 \pm 1.44%
I+P	P	64.55 \pm 1.93%	I+P	P	64.12 \pm 2.38%	I+P	P	64.37 \pm 2.14%
I+P	I+P	69.04 \pm 2.01%	I+P	I+P	68.90 \pm 2.27%	I+P	I+P	69.14 \pm 1.75%

Table 15: Full results, LAB + UTO \rightarrow SEA, InfoNCE

EfficientNet B0 + CNN			ConvNeXt Femto + CNN			ViT-Tiny + CNN		
Gallery	Test	Accuracy	Gallery	Test	Accuracy	Gallery	Test	Accuracy
I	I	68.46 \pm 2.94%	I	I	67.77 \pm 1.93%	I	I	66.23 \pm 1.84%
I	P	30.21 \pm 3.37%	I	P	39.02 \pm 4.02%	I	P	32.42 \pm 4.50%
I	I+P	68.44 \pm 3.23%	I	I+P	68.57 \pm 2.21%	I	I+P	66.24 \pm 2.02%
P	I	37.15 \pm 4.03%	P	I	37.57 \pm 2.92%	P	I	32.56 \pm 4.59%
P	P	64.07 \pm 2.92%	P	P	64.32 \pm 2.29%	P	P	65.36 \pm 2.57%
P	I+P	65.11 \pm 3.03%	P	I+P	65.25 \pm 2.28%	P	I+P	65.92 \pm 2.86%
I+P	I	68.39 \pm 2.96%	I+P	I	67.69 \pm 1.93%	I+P	I	66.25 \pm 1.86%
I+P	P	64.07 \pm 2.92%	I+P	P	64.32 \pm 2.28%	I+P	P	65.34 \pm 2.57%
I+P	I+P	71.05 \pm 2.87%	I+P	I+P	71.77 \pm 2.42%	I+P	I+P	71.37 \pm 2.17%
EfficientNet B0 + Transformer			ConvNeXt Femto + Transformer			ViT-Tiny + Transformer		
Gallery	Test	Accuracy	Gallery	Test	Accuracy	Gallery	Test	Accuracy
I	I	70.25 \pm 2.22%	I	I	68.25 \pm 1.57%	I	I	68.86 \pm 1.39%
I	P	42.30 \pm 4.78%	I	P	44.25 \pm 6.44%	I	P	37.49 \pm 3.54%
I	I+P	70.86 \pm 2.34%	I	I+P	69.43 \pm 1.89%	I	I+P	70.06 \pm 1.71%
P	I	35.81 \pm 3.41%	P	I	28.65 \pm 4.78%	P	I	33.44 \pm 1.87%
P	P	66.00 \pm 2.28%	P	P	65.93 \pm 2.15%	P	P	66.37 \pm 1.64%
P	I+P	66.51 \pm 2.28%	P	I+P	66.15 \pm 2.31%	P	I+P	66.97 \pm 1.68%
I+P	I	70.24 \pm 2.22%	I+P	I	68.25 \pm 1.57%	I+P	I	68.86 \pm 1.39%
I+P	P	66.00 \pm 2.28%	I+P	P	65.93 \pm 2.15%	I+P	P	66.37 \pm 1.64%
I+P	I+P	72.13 \pm 2.03%	I+P	I+P	71.67 \pm 1.53%	I+P	I+P	72.73 \pm 1.20%

Table 16: Full results, LAB + UTO \rightarrow SEA, InfoNCE

EfficientNet B4 + CNN			ConvNeXt Tiny + CNN			ViT-Small + CNN		
Gallery	Test	Accuracy	Gallery	Test	Accuracy	Gallery	Test	Accuracy
I	I	73.60 \pm 2.23%	I	I	70.87 \pm 2.74%	I	I	72.40 \pm 2.31%
I	P	36.73 \pm 3.04%	I	P	35.77 \pm 3.06%	I	P	41.15 \pm 4.36%
I	I+P	73.99 \pm 2.11%	I	I+P	70.93 \pm 3.08%	I	I+P	72.59 \pm 2.54%
P	I	38.81 \pm 3.51%	P	I	33.65 \pm 2.89%	P	I	42.56 \pm 2.51%
P	P	65.19 \pm 2.31%	P	P	66.26 \pm 2.37%	P	P	65.78 \pm 2.42%
P	I+P	66.19 \pm 2.27%	P	I+P	66.87 \pm 2.47%	P	I+P	66.73 \pm 2.34%
I+P	I	73.59 \pm 2.23%	I+P	I	70.63 \pm 2.76%	I+P	I	72.19 \pm 2.35%
I+P	P	65.19 \pm 2.31%	I+P	P	66.25 \pm 2.36%	I+P	P	65.79 \pm 2.40%
I+P	I+P	74.94 \pm 2.33%	I+P	I+P	73.77 \pm 2.24%	I+P	I+P	72.75 \pm 2.04%
EfficientNet B4 + Transformer			ConvNeXt Tiny + Transformer			ViT-Small + Transformer		
Gallery	Test	Accuracy	Gallery	Test	Accuracy	Gallery	Test	Accuracy
I	I	73.48 \pm 2.79%	I	I	68.16 \pm 1.98%	I	I	69.74 \pm 1.65%
I	P	40.15 \pm 4.22%	I	P	44.68 \pm 3.51%	I	P	39.61 \pm 5.15%
I	I+P	72.81 \pm 2.45%	I	I+P	69.00 \pm 2.05%	I	I+P	70.66 \pm 1.87%
P	I	43.98 \pm 2.97%	P	I	36.60 \pm 2.65%	P	I	35.57 \pm 3.27%
P	P	66.11 \pm 3.19%	P	P	67.27 \pm 2.85%	P	P	66.50 \pm 1.83%
P	I+P	66.71 \pm 3.26%	P	I+P	67.50 \pm 3.00%	P	I+P	66.99 \pm 1.82%
I+P	I	73.43 \pm 2.78%	I+P	I	68.08 \pm 2.00%	I+P	I	69.69 \pm 1.65%
I+P	P	66.11 \pm 3.18%	I+P	P	67.28 \pm 2.84%	I+P	P	66.50 \pm 1.83%
I+P	I+P	71.78 \pm 2.99%	I+P	I+P	71.74 \pm 2.39%	I+P	I+P	71.04 \pm 1.40%